Calculation of Solvent Shifts on Electronic g-Tensors with the Conductor-Like Screening Model (COSMO) and Its Self-Consistent Generalization to Real Solvents (Direct COSMO-RS)

Sebastian Sinnecker,[†] Arivazhagan Rajendran,[†,‡] Andreas Klamt,[§] Michael Diedenhofen,[§] and Frank Neese*[,†]

Max-Planck-Institut für Bioanorganische Chemie, Stiftstrasse 34-36, D-45470 Mülheim an der Ruhr, Germany, COSMOlogic GmbH&Co.KG, Burscheider Strasse 515, D-51381 Leverkusen, Germany

Received: October 20, 2005; In Final Form: December 21, 2005

The conductor-like screening model (COSMO) was used to investigate the solvent influence on electronic *g*-values of organic radicals. The previously studied diphenyl nitric oxide and di-*tert*-butyl nitric oxide radicals were taken as test cases. The calculations employed spin-unrestricted density functional theory and the BP and B3LYP density functionals. The **g**-tensors were calculated as mixed second derivative properties with respect to the external magnetic field and the electron magnetic moment. The first-order response of the Kohn−Sham orbitals with respect to the external magnetic field was determined through the coupled-perturbed DFT approach. The spin−orbit coupling operator was treated using an accurate multicenter spin−orbit mean-field (SOMF) approach. Provided that important hydrogen bonds are explicitly modeled by a supermolecule approach and that the basis set is sufficiently saturated, the COSMO calculations lead to accurate predictions of isotropic *g*-shifts with deviations of not more than 100 ppm relative to experiment. Very accurate results were obtained by employing a recently developed self-consistent modification of the COSMO method to real solvents (COSMO-RS), which we briefly introduce in this paper as direct COSMO-RS (D-COSMO-RS). This model gives isotropic *g*-shifts of similar high accuracy for water without using the supermolecule approach. This is an important result because it solves many of the problems associated with the supermolecule approach such as local minima and the choice of a suitable model system. Thus, the self-consistent D-COSMO-RS incorporates some specific solvation effects into continuum models, in particular it appears to successfully model the effects of hydrogen bonding. Although not yet widely validated, this opens a novel approach for the calculation of properties which so far only could be calculated by the inclusion of explicit solvent molecules in continuum solvation methods.

1. Introduction

The vast majority of chemical experiments is performed in condensed media, i.e., in solutions or in solids. Thus, a modeling of the interaction of the solute with its surrounding at some level of sophistication is necessary to accurately predict molecular properties and energetics. In particular, the influence of solvent effects on various kinds of molecular optical and magnetic spectra can be fairly pronounced.[1] A number of strategies at different levels of sophistication have been used in quantum chemistry for taking these influences into account. An alternative approach is the use of ab initio molecular dynamics simulations, for example, within the Car−Parrinello method.[2] However, such an approach may become computationally fairly expensive, especially as the number of solvent molecules that are explicitly considered becomes large. If the dynamics of the system are neglected, the approach reduces to a standard quantum chemical calculation within a supermolecule approach in which the solvent and solute are treated on equal footing. However, the number of solvent molecules that can be treated is limited due to excessive computer resource requirements, and truly long-range interactions cannot be modeled in this way. Alternatively, a fairly large number of solvent molecules can be considered in mixed classical/quantum mechanical (QM/MM) approaches combined with appropriate sampling and dynamics techniques.[3−6] Such approaches are increasingly popular and aim at an atomistic simulation of the entire system of solute and solvent. However, in many instances, the major effects of solvation can already be captured using much simpler and computationally efficient continuum dielectric approaches,[7−9] such as the polarizable continuum model (PCM),[10] or the conductor like screening approach (COSMO).[11] The latter method is the focus of this paper.

In the continuum dielectric approaches, the solute is placed in a cavity of some kind and interacts with an unstructured but polarizable continuum that is mainly characterized through its dielectric constant. Different approaches appeared for the construction of the shape of this cavity, ranging from spherical cavities to more elaborate solvent accessible and solvent excluding surfaces.[12] Likewise, different approaches were developed for the treatment of the electrostatic interaction between the solute and the continuum. On one hand, multipole expansions allow for the construction of the molecular and solvent potentials.[13,14] Alternatively, the potentials can be described by introducing a charge distribution on the cavity surface.[10,11] In principle, both formalisms can exactly describe

* Corresponding author. E-mail: Neese@mpi-muelheim.mpg.de.
[†] Max-Planck-Institut für Bioanorganische Chemie.
[‡] Present address: Chemical Laboratory, Central Leather Research Institute (CSIR), Adyar, Chennai, India 600 020.
[§] COSMOlogic GmbH&Co.KG.

10.1021/jp056016z CCC: $33.50
Published on Web 01/25/2006

CHART 1: Molecular Structures of the Diphenyl Nitric Oxide (DPNO) and Di-*tert*-butyl Nitric Oxide (DTBNO) Radicals, and the g-Tensor Orientation[a]

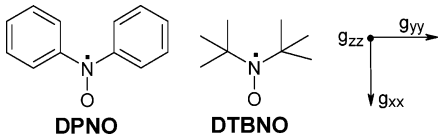

[a] The largest component g_{xx} points along the N−O bond.

the electrostatic interaction between the solute and the continuum. Furthermore, other interaction terms such as dispersion interactions can be introduced into continuum models.[8]

The general advantage of continuum models is that they do not increase the number of the degrees of freedom of the investigated systems, which keeps the computational effort small.[8] However, the supermolecule approach has been considered as the method of choice for the description of specific interactions such as solvent to metal ion coordination, hydrogen bonding or spin density transfer, because these effects cannot be described by continuum models.[15−22] In the case of polar, protic solvents, the combination of continuum models with explicit treatment of a few important solvent molecules by a supermolecule approach has recently been shown to be a successful compromise between computational cost and accuracy.[23,24] Applications of continuum models range from structural and energetic considerations to the calculation of absorption spectra,[25−27] NMR chemical shifts and spin−spin coupling constants,[5,28,29] EPR hyperfine coupling constants and **g**-tensors.[23,24,30−33] In particular, the dependence of molecular *g*-values on the solvent polarity is widely used in various research communities to obtain information on the environment of radical spin-labels that can be specifically attached, e.g., to protein sites to study conformational changes or even folding processes.[34−36]

Solvent effects on electronic **g**-tensors have previously been treated together with the PCM model by Ciofini et al.,[23,29,30] as well as in a recent study of Rinkevicius et al.[24] Although in the study of Ciofini et al. the solvent effect on the **g**-tensor shows up through the use of "solvated" orbitals and orbital energies, Rinkevicius et al. contended that there are contributions of the solvent potential to the response equations. The work on the glycyl radical of Ciofini et al. additionally provided a careful comparison of the performance of different functionals and basis sets with respect to the accurate calculation of hyperfine coupling constants and **g**-tensors.[30]

In the present work, we focus on the use of the COSMO model to describe bulk solvent effects on **g**-tensors which, to the best of our knowledge, has not been done before. In addition, our approach is extended to the self-consistent formulation of the COSMO model for real solvents (D-COSMO-RS).[37] To allow a fair comparison of our approach to the work of Rinkevicius et al.,[24] we have used the same test molecules and basis sets as in their study. The chosen model systems are diphenyl nitric oxide (DPNO) and di-*tert*-butyl nitric oxide (DTBNO), which are shown in Chart 1. The considered solvents range from aprotic apolar fluids such as tetrachloromethane to highly protic and polar solvents such as water. The quality of the calculated **g**-tensors is judged by a comparison with the experimental results. The EPR properties of both radicals in different solvents were studied already in early work: though the DPNO radical was the subject of matter in a long series of papers,[38−44] there is only one experimental study on the DTBNO radical available so far.[45] Due to the similarity of these systems to nitric oxide spin label compounds, our study should additionally gain importance; the tremendous value of spin labels in EPR studies is underlined by several computational studies on nitric oxide spin labels and related model systems.[46−50]

2. Theory

EPR *g*-values describe the interaction of the molecular magnetic dipole moment with the external magnetic field (molecular Zeeman effect). Following the modern philosophy of evaluating properties as derivatives of the total energy computed with some quantum mechanical method, the **g**-tensor is calculated as a mixed second-derivative with respect to the external magnetic field and the electron magnetic moment.[51−54] The response of the system to the external magnetic field within a DFT or Hartree−Fock framework is determined through the coupled-perturbed self-consistent field (CP−SCF) equations.

The **g**-matrix can be divided into the following contributions ($p, q = x, y, z$):[51]

$$g_{pq} = g_e\delta_{pq} + \Delta g^{\mathrm{RMC}}\delta_{pq} + \Delta g^{\mathrm{DSO}}_{pq} + \Delta g^{\mathrm{PSO}}_{pq} \qquad (1)$$

The first isotropic term is given by the free electron *g*-value g_e. The second and third contributions refer to the first-order relativistic mass and diamagnetic spin−orbit terms (previously referred to as "gauge correction") and can be straightforwardly calculated from the kinetic energy integrals and the spin density.[51] The last term in eq 1 is the paramagnetic spin−orbit term (or orbital Zeeman/spin−orbit coupling cross term) and is dominant in almost all cases. This term can be expressed as

$$\Delta g^{\mathrm{PSO}}_{p,q} = -\frac{1}{2S}\sum_{\mu,\nu}\frac{\partial P^{\alpha-\beta}_{\mu\nu}}{\partial B_p}\langle\varphi_\mu|\hat{h}^{\mathrm{SO}}_q|\varphi_q\rangle \qquad (2)$$

Here, S is the total spin of the system, $P^{\alpha-\beta}_{\mu\nu}$ is the μ,νth element of the spin-density matrix $\mathbf{P}^{\alpha-\beta} = \mathbf{P}^{\alpha} - \mathbf{P}^{\beta}$ in the basis of atomic orbitals $\{\varphi\}$. The operator $\hat{h}^{\mathrm{SO}}_q$ is the qth component of the spatial part of an effective one-electron spin−orbit coupling (SOC) operator and B_p is the pth component of the external magnetic field. The derivative of the spin-density matrix with respect to the external magnetic field is calculated from the solution of the CP−SCF equations.[51] Given, the skew-symmetric matrix **U** of ref 51 in the MO basis,

$$\frac{\partial P^{\alpha-\beta}_{\mu\nu}}{\partial B_p} = [\mathbf{c}^{\alpha}\mathbf{U}^{\alpha(p)}\mathbf{c}^{\alpha T} - \mathbf{c}^{\beta}\mathbf{U}^{\beta(p)}\mathbf{c}^{\beta T}]_{\mu\nu} \qquad (3)$$

where $\mathbf{c}^{\sigma}$ are the MO-coefficients for spin-σ.

In the present work, the operator $\hat{h}^{\mathrm{SO}}_q$ is treated by an accurate mean-field (SOMF) approximation to the full Breit−Pauli SOC operator. The SOMF approach has been developed by Hess et al.[55] It is widely used within Schimmelpfennig's AMFI program in a number of quantum chemistry codes.[56,57] However, it introduces two further approximations which are (a) the neglect of multicenter SOC terms and (b) the use of atomic self-consistent field orbitals and their averaged occupation numbers in place of the molecular charge densities. Both approximations were introduced in the interest of computational efficiency and their justification is through the successful molecular test calculations.[57]

We have recently discussed an efficient implementation of the SOMF concept, which is based on the following formulation of the effective one-electron operator:[58,59]

$$\langle\varphi_\mu|\hat{h}_p^{SOC}|\varphi_\nu\rangle = \langle\varphi_\mu|\hat{h}_p^{1el-SOC}|\varphi_\nu\rangle + \sum_{\kappa\tau}P_{\kappa\tau}\left[(\varphi_\mu\varphi_\nu|\hat{g}_p^{SOC}|\varphi_\kappa\varphi_\tau) - \frac{3}{2}(\varphi_\mu\varphi_\kappa|\hat{g}_p^{SOC}|\varphi_\tau\varphi_\nu) - \frac{3}{2}(\varphi_\tau\varphi_\nu|\hat{g}_p^{SOC}|\varphi_\mu\varphi_\kappa)\right] \quad (4)$$

with the one- and two-electron operators:

$$\hat{h}_p^{1el-SOC}(\mathbf{r}_i) = \frac{\alpha^2}{2}\sum_i\sum_A Z_A r_{iA}^{-3}\hat{\mathbf{l}}_{iA;p} \quad (5a)$$

$$\hat{g}_p^{SOC}(\mathbf{r}_i,\mathbf{r}_j) = -\frac{\alpha^2}{2}\hat{\mathbf{l}}_{ij;p}r_{ij}^{-3} \quad (5b)$$

Here, **P** is the total charge density matrix, α is the fine structure constant, Z_A is the nuclear charge of atom A, r_{iA} is the position of electron i relative to nucleus A and $\hat{\mathbf{l}}_{iA;p}$ is the pth component of the angular momentum of the ith electron relative to atom A. Likewise, r_{ij} is the distance between electrons i and j and $\hat{\mathbf{l}}_{ij;p}$ is the pth component of the angular momentum of electron i relative to electron j. The one-electron term of the SOMF approximation (the first term in eq 4) is treated exactly. The two electron part of the SOMF Hamiltonian features a Coulomb term (the first term in the summation in eq 4), which is very efficiently and accurately approximated through the resolution of the identity (RI) approximation in our approach, whereas the much smaller exchange terms (the last two terms in eq 4) are treated within a one-center approximation. This is referred to as the RI-SOMF(1X) SOC operator. It should be noted that in the SOMF approach the spin-same-orbit and spin-other-orbit contributions as well as exchange effects are fully treated to a very good approximation. This is not the case for the widely used SOC operators which are derived from the local DFT potential because they do not consider the important spin-other orbit contributions[53] and introduce an exchange part of the wrong sign.[58]

The conductor-like screening model (COSMO) is a continuum solvation model that was introduced by Klamt and Schüürmann.[11] Within this model, the continuum is initially assumed to be a perfect conductor that completely screens the charge density of the solute. After determination of the screening charges, they are scaled down to a finite dielectric constant and implemented in the Hamiltonian of the system. The screening charges are calculated for realistic, van der Waals-like molecular cavities. The availability of analytic gradients allows also for an geometry optimization of the solute within the continuum.

Within the COSMO approach, there is a contribution to the Fock- or Kohn−Sham matrix of the form

$$V_{\mu\nu}^{COSMO} = f(\epsilon)\cdot\sum_t q_t\left\langle\varphi_\mu\left|\frac{1}{\mathbf{r}-\mathbf{r}_t}\right|\varphi_\nu\right\rangle \quad (6)$$

where $f(\epsilon) = \epsilon - 1/\epsilon + {}^1/_2$ and ϵ is the dielectric constant of the solvent and the sum is performed over surface segments t with screening charge q_t at positions $\mathbf{r}_t$. The screening charges are calculated from

$$\mathbf{q} = -\mathbf{A}^{-1}\phi \quad (7)$$

where the **A**-matrix is explained elsewhere,[11] and the potential created by the molecular charge distribution on surface segment t is

$$\phi_t = \int\frac{\rho_{el}(\mathbf{r}) + \rho_{Nuc}(\mathbf{r})}{|\mathbf{r}-\mathbf{r}_t|}\,d\mathbf{r} \quad (8)$$

with

$$\rho_{el}(\mathbf{r}) + \rho_{Nuc}(\mathbf{r}) = -\sum_{\mu\nu}P_{\mu\nu}\varphi_\mu(\mathbf{r})\,\varphi_\nu(\mathbf{r}) + \sum_A Z_A\delta(\mathbf{r}-\mathbf{R}_A) \quad (9)$$

The total free energy of the solvated molecule is the sum of the energy of the isolated system calculated with the solvated wave function and the so-called dielectric energy, which is the free electrostatic energy gained by the solvation process

$$E^{diel} = \frac{1}{2}f(\epsilon)\sum_t q_t\phi_t \quad (10)$$

The important point is that the COSMO contribution to the SCF operator is a local functional of the total charge density. Thus, in the first-order SCF equations, the derivative of the COSMO term with respect to an external perturbation λ becomes[60]

$$\frac{\partial V^{COSMO}[\rho]}{\partial\lambda} = \int\frac{\delta V^{COSMO}[\rho]}{\delta\rho(\mathbf{r})}\frac{\partial\rho(\mathbf{r})}{\partial\lambda}\,d\mathbf{r} \quad (11)$$

However, as long as the basis functions do not depend on the perturbation and the perturbation is purely imaginary (i.e., of the magnetic field type), we have

$$\frac{\partial\rho(\mathbf{r})}{\partial\lambda} = 0 \quad (12)$$

This shows there is no explicit contribution of the COSMO terms to the magnetic field response equations and thus, the entire solvent effect is contained in its effect on the calculated geometries, orbital shapes and orbital energies.

An extension of the COSMO approach to real solvents (COSMO-RS) was developed to overcome many of the limitations of the dielectric continuum solvation concept and allows for the reliable and predictive treatment of almost arbitrary solutes and in almost arbitrary solvents and mixtures at variable temperature.[37,61] In the normal COSMO-RS concept, the quantum chemical COSMO calculations for solutes and solvents are always performed for a perfect conductor as pseudo-solvent ($\epsilon = \infty$). This state is used as a reference state. In a next step, we imagine a liquid mixture as a dense packing of molecules in the reference state. The surface interaction energy modes, i.e., the electrostatic deviations from the conductor limit electrostatics (E_{misfit}) and hydrogen bonding (E_{HB}), are described as functions of the screening charge densities ($\sigma = q/a$) of two interacting surface segments σ and σ' or $\sigma_{acceptor}$ and σ_{donor}, if the segments are located on a hydrogen bond donor or acceptor atom.

$$E_{misfit}(\sigma,\sigma') = a_{eff}\frac{\alpha'}{2}(\sigma+\sigma')^2 \quad (13)$$

$$E_{HB} = a_{eff}c_{HB}\min(0;\min(0;\sigma_{donor}+\sigma_{HB})\max(0;\sigma_{acceptor}-\sigma_{HB})) \quad (14)$$

Equations 13 and 14 contain five adjustable parameters, an interaction parameter α', the effective contact area a_{eff}, the hydrogen bond strength c_{HB}, and the threshold for hydrogen bonding σ_{HB}. The less specific van der Waals (E_{vdW}) interactions

are taken into account in a slightly more approximate way by element specific interaction terms.[63]

Because all interactions are defined by the element type and σ, the required information on the molecular surface of compound i can be covered by a distribution-function, the so-called σ-profile $p^i(\sigma)$, which gives the relative amount of surface with polarity σ. The σ-profile for the entire solvent of interest $p_S(\sigma)$can be expressed as the sum of all components weighted by their mole fraction

$$p_S(\sigma) = \sum_{i \in S} x_i p^i(\sigma) \tag{15}$$

Using this profile and the total interaction energy E_{int}, which is the sum of the interaction terms discussed above, the chemical potential of the surface segments can be calculated solving a coupled set of nonlinear equations.

$$\mu_S(\sigma;T) = -\frac{RT}{a_{\text{eff}}} \ln\left[\int p_S(\sigma') \exp\left(\frac{a_{\text{eff}}}{RT}(\mu_S(\sigma';T) - E_{\text{int}}(\sigma,\sigma'))\right) \mathrm{d}\sigma'\right] \tag{16}$$

The function $\mu_S(\sigma;T)$, called σ-profile hereafter, gives a measure for the affinity of the system S to a surface of polarity σ. Thus, it allows for the calculation of the chemical potential of a compound i in the defined mixture

$$\mu_S^i = \mu_{C,S}^i + \int p^i(\sigma)\, \mu_S(\sigma;T)\, \mathrm{d}\sigma + kT \ln(x_i) \cong \sum_{t=1}^{m} a_t\, \mu_S(\sigma_t;T) + \mu_{C,S}^i + kT \ln(x_i) \tag{17}$$

where the combinatorial term $\mu_{C,S}^i$ accounts for effects arising from the size and shape differences of the molecules in the mixture.

A more detailed discussion and an example parameter set can be found in refs 61 and 63.

Although this concept has proven to be very successful for the calculation of chemical potentials and equilibrium constants, it is not capable of providing any information about the response of the solute wave function on the presence of a specific solvent, and hence it cannot be used for the prediction of specific solvation effects on many molecular properties as geometries, dipole moments, absorption spectra, vibrational frequencies, etc. Technically, these properties can be treated on the continuum dielectric solvation level, but this level is theoretically inappropriate at least for polar solvents, and it is unable to take into account specific hydrogen bonding interactions. Thus the extension of the COSMO-RS method to a self-consistent domain in which the COSMO-RS response function is directly fed into the quantum chemical wave function is necessary. Because this method will avoid the indirect calculations by a conductor-SCF followed by post-SCF COSMO-RS, we shall call this approach "Direct COSMO-RS" or D-COSMO-RS. This approach was recently implemented in ORCA and is tested here for the first time. A more detailed paper on D-COSMO-RS will be published soon.

For a short derivation of the D-COSMO-RS theory, let us consider the calculation of a solute i in a pure or mixed solvent S, and let us assume that we already know the σ-potential $\mu_S(\sigma;T)$ (eq 16) of the solvent S from prior COSMO-RS calculations. Then the COSMO-RS expression for the free energy of the molecule in a solvent S is defined by eq 17 and the corresponding solvent operator of the system can be derived by functional derivation of the solute−solvent interaction energy with respect to the electron density. Because the full interaction energy is the sum of the dielectric energy of the COSMO model (eq 10) and the free energy in solution from eq 17, the solvation operator of the D-COSMO-RS model reads

$$\hat{V}^{\text{RS}} = -\sum_t \frac{q_t + q_t^{\Delta\text{RS}}}{|\mathbf{r}_t - \mathbf{r}|} \tag{18}$$

The real solvation influence defined by the COSMO-RS theory correction $q_t^{\Delta RS}$ results from the potential

$$\phi_{\text{t}}^{\Delta\text{RS}} = a_t \left(\frac{\delta \mu_S}{\delta q}\right)_{q=q_t} \tag{19}$$

and eq 7.

Thus, the solvation influence of the COSMO-RS model can be viewed as a correction of the ideal screening charges appearing in a conductor.

3. Computational Details

All calculations were performed with the quantum chemical program package ORCA.[62] The COSMO method was recently efficiently implemented into the ORCA program including the self-consistent generalization of the COSMO-RS model. It was successfully tested in the calculation of solvent shifts on electronic spectra, which will be reported in a forthcoming publication.

Solvents. The following solvents with their dielectric constants ϵ in parentheses were considered in this work: tetrachloromethane (TCL; 2.24), toluene (2.4), acetone (20.7), acetonitrile (36.6), methanol (32.63), and water (80.4). The COSMO-RS potentials needed for the D-COSMO-RS approach have been derived with the COSMO*therm* program using the BP_TZVP C21_0104 parametrization at 25 °C and infinite dilution of the solute.[63,64]

Geometry Optimizations. The molecular structures of the radicals DPNO and DTBNO (Chart 1) were completely geometry optimized by employing density functional theory (DFT) and the COSMO continuum model. Unrestricted calculations were performed employing the B3LYP hybrid DFT method.[65,66] In all cases, the 6-31G(d,p) basis sets were used.[67,68] Additionally, explicit solvent molecules were added to the radicals DPNO and DTBNO to describe hydrogen bonding effects in case of methanol and water. These complexes were completely geometry optimized either in a vacuum or with inclusion of the COSMO terms. All geometry optimizations were carried out in redundant internal coordinates as implemented in the ORCA program. Geometries were considered converged when the following parameters were below their thresholds given in parentheses: energy change (5×10^{-6} E_{h}), maximum gradient (3×10^{-4} E_{h}/bohr), RMS gradient (1×10^{-4} E_{h}/bohr), maximum displacement (4×10^{-3} bohr), and RMS displacement (2×10^{-3} bohr).

Calculation of g-Tensors. The **g**-tensor calculations were performed as described in the previous section. The calculated g-values g_{ii} ($i = x, y, z$) are given as g-shifts Δg_{ii} in parts per million (ppm) with $\Delta g_{ii} = 10^6 \times (g_i - g_e)$, where $g_e = 2.002\,319$ is the free electron g-value. The isotropic g-value is defined as one-third of the sum of the principal g-values.

All **g**-tensor calculations were performed by employing the BP[69−71] and B3LYP functionals, together with the IGLO-II basis set for all atoms.[72] To investigate the accessible accuracy of

the calculated *g*-shifts with respect to larger basis sets, a comparison of experimental and calculated isotropic *g*-shifts is additionally given in this study by employing the IGLO-III basis functions.[72] Furthermore, a single set of diffuse functions was added for H, N, and O, that is, an s-function for hydrogen and p-functions for the other elements. The exponents were chosen to be one-third of the smallest exponent in the respective shell.

The present calculations do not employ gauge including atomic orbitals (GIAO's) and the results are therefore dependent on the choice of origin. However, employing the IGLO-II basis sets, we found only a negligible dependency of the *g*-shifts on the gauge origin: COSMO calculations on the DPNO radical in coordination with two water molecules gave *g*-shifts within 1 ppm of each other for gauge origins (a) at the center of the electronic charge (our default),[73] (b) at the center of the nuclear charge, and (c) at the center of mass.

4. Results and Discussion

Nature of the g-Tensor and Solvent Effects on It. In general, the **g**-tensor of organic radicals can be explained with help of the Stone's theory.[74,75] Heteroatoms such as oxygen or nitrogen can carry a large amount of spin density in these systems and lead to a distinct **g**-tensor anisotropy. This is on one hand the consequence of the noticeable spin−orbit mixing due to the large spin−orbit coupling constants of the heteroatoms, and on the other hand due to the existence of nonbonding orbitals that are energetically close to the semi occupied molecular orbital (SOMO). For nitroxide radicals, three *g*-shifts of different magnitudes are expected with $\Delta g_{xx} > \Delta g_{yy} > \Delta g_{zz}$, and Δg_{zz} close to zero, $g_{zz} \approx g_e$. Especially the large g_{xx} shift, with an eigenvector pointing along the N−O direction (Chart 1), is a very sensitive probe for the polarity of the surrounding.[24] The most important contribution to Δg_{xx} results from an electronic excitation from the in-plane lone pair SOMO−1 orbitals to the out of plane π^* SOMO orbitals (Figure 1). A noticeable, but decreased, sensitivity on the solvent was found for the Δg_{yy} component, whereas the g_{zz} component, which is oriented perpendicular to the R_2N-O plane (Chart 1), is almost independent of the polarity of the surrounding.

The influence of the solvent polarity on the calculated *g*-shifts is the result of a stabilization of the in-plane lone-pair orbitals of the radicals in more polar solvents. This interaction increases the energy gaps between the in-plane lone pair orbitals and the semi-occupied molecular orbitals and lowers especially the g_{xx} shift. In this work, this effect was reproduced by calculations with a stepwise increased dielectric constant ϵ (Figure 2). Employing the B3LYP functional and the IGLO-II basis set, the following differences in the *g*-shifts were observed between gas-phase calculations and calculations in water ($\epsilon = 80.4$): $\Delta\Delta g_{xx} = 722$ ppm, $\Delta\Delta g_{yy} = 140$ ppm, $\Delta\Delta g_{zz} = 9$ ppm for the DPNO radical and $\Delta\Delta g_{xx} = 443$ ppm, $\Delta\Delta g_{xx} = 108$ ppm, $\Delta\Delta g_{zz} = 12$ ppm for the DTBNO radical. The different values for the isotropic *g*-shifts Δg_{iso} that were measured in the experiments or calculated in this work can therefore be traced back to the changes in Δg_{xx} and to a lower extent also to Δg_{yy}, whereas Δg_{zz} remains almost constant.

Besides this purely electrostatic interaction, the formation of hydrogen bonds to the radicals leads to a stabilization of the lone-pair orbitals. This lowers especially the g_{xx} shift.

All these aspects are not only valid for the two investigated nitric oxide radicals, DPNO and DTBNO but also are in qualitative agreement with our analysis of the **g**-tensor for the benzosemiquinone radical anion in protic solvents,[22] which was confirmed by high field EPR experiments in frozen solutions.[76]

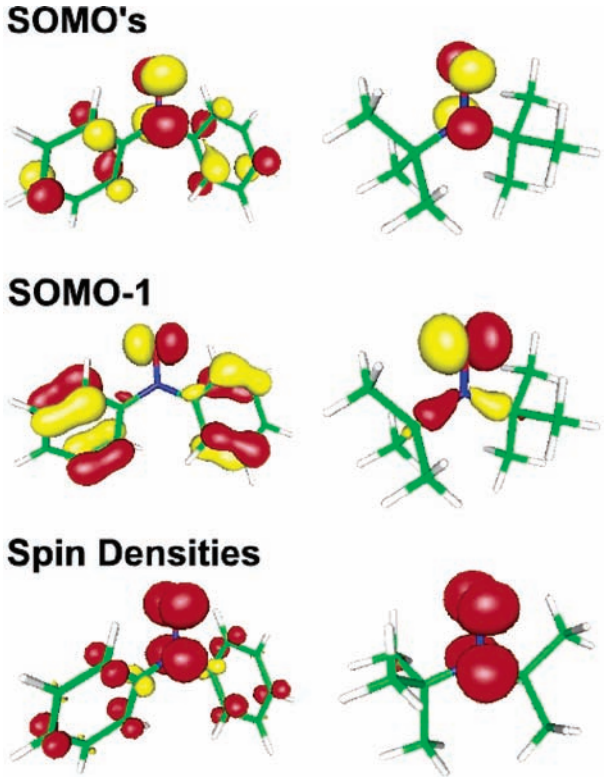

Figure 1. Semioccupied molecular orbitals (SOMO's), the doubly occupied SOMO−1 orbitals and the spin densities of the DPNO (left) and DTBNO radicals (right). The SOMO's give an impression of the delocalization of the unpaired electron in these systems. The dominating Δg_{xx} shift is mainly the result of an electronic excitation from the SOMO−1 level to the SOMO orbitals.

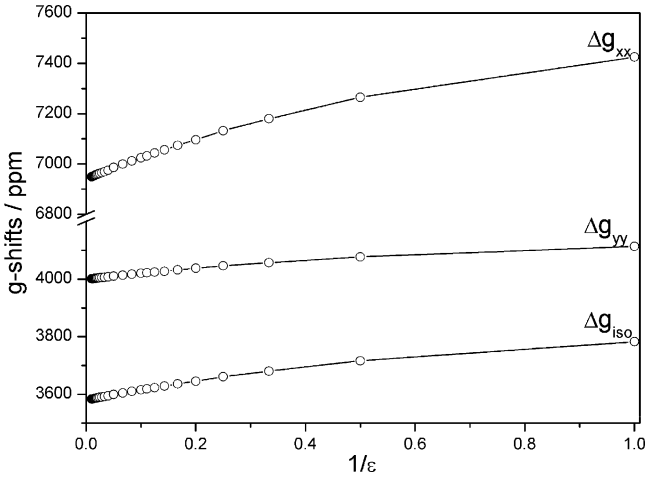

Figure 2. Calculated *g*-shifts of the DTBNO radical as a function of $1/\epsilon$ with ϵ being the dielectric constant (COSMO, B3LYP//B3LYP). The very small Δg_{zz} shifts (−191 ppm for $\epsilon = 1$ and −200 ppm for $\epsilon = 100$) are not displayed.

Knüpling et al. have shown that a multipole expansion with monopole−monopole, monopole−dipole, dipole−dipole, and dispersion contributions can be used to describe the electrostatic potential around the solute, which makes an interpretation of the **g**-tensor dependence on hydrogen bond lengths possible.[77]

In the following paragraphs, a more quantitative and more detailed discussion of these general effects is given for the two nitroxide radicals from Chart 1.

COSMO Calculations for Systems without Explicit Solvent Molecules. Geometry optimizations of the DPNO and

TABLE 1: Calculated *g*-Shifts (ppm) for the Diphenyl Nitric Oxide Radical DPNO (Chart 1) Using Solvent Optimized Geometries

	BP				B3LYP				exptl[40]
solvent	Δg_{xx}	Δg_{yy}	Δg_{zz}	Δg_{iso}	Δg_{xx}	Δg_{yy}	Δg_{zz}	Δg_{iso}	Δg_{iso}
vacuum	6866	2861	−71	3219	7656	3337	−101	3631	
TCL	6678	2827	−68	3146	7386	3290	−98	3526	3401 ± 10
toluene	6664	2825	−67	3140	7366	3286	−98	3518	
acetone	6389	2772	−62	3033	6984	3215	−93	3369	
acetonitrile	6366	2768	−61	3024	6951	3209	−92	3356	
methanol	6362	2766	−61	3022	6949	3208	−92	3355	3181 ± 10
water	6345	2763	−61	3016	6924	3203	−92	3345	2761 ± 10

TABLE 2: Calculated *g*-Shifts (ppm) for the Di-*tert*-butyl Nitric Oxide Radical DTBNO (Chart 1) Using Solvent Optimized Geometries

	BP				B3LYP				exptl[45]
solvent	Δg_{xx}	Δg_{yy}	Δg_{zz}	Δg_{iso}	Δg_{xx}	Δg_{yy}	Δg_{zz}	Δg_{iso}	Δg_{iso}
vacuum	6635	3734	−174	3399	7402	4114	−198	3773	
TCL	6528	3702	−170	3353	7236	4074	−194	3705	3751 ± 20
toluene	6525	3700	−170	3351	7228	4071	−195	3701	3741 ± 10
acetone	6411	3659	−179	3297	7032	4014	−204	3614	3721 ± 50
acetonitrile	6357	3658	−170	3282	6971	4013	−196	3596	3651 ± 10
methanol	6359	3651	−176	3278	6972	4005	−201	3592	3471 ± 20
water	6354	3651	−174	3277	6964	4005	−199	3590	3241 ± 10

DTBNO radicals were performed including the COSMO correction. However, the choice of solvent had only a very small effect on the calculated structure parameters. This is an important point because already small changes in the geometry of the radicals, especially of the N−O bond distances, can noticeably influence the **g**-tensors of the systems.[46] For example, the N−O distances in DPNO in a vacuum and in H_2O are calculated to be 1.286 and 1.290 Å, respectively. Slightly larger changes were found for bond and dihedral angles.

The calculated *g*-shifts for the DPNO and DTBNO radicals are given in Tables 1 and 2, respectively. A comparison of the calculated and experimental *g*-shifts is somewhat hindered by the fact that only a limited number of measured data are available for these species. The **g**-tensor anisotropy has not been resolved so far for both species in the experiments, which would require the use of high-field EPR methods at low temperatures in frozen solutions. Isotropic *g*-values were obtained in EPR studies on the DPNO radical in tetrachloromethane (TCL), methanol and water.[40] For the DTBNO radical, isotropic *g*-values were measured in all solvents that were used in this study.[45] In general, the DPNO radical with its extended π-electron system and increased spin density delocalization (Figure 1) shows smaller g_{iso} shifts than the DTBNO radical with its alkyl substituents, which is well recovered in the calculations.

For both nitric oxide radicals, DPNO and DTBNO, the experimental trend to smaller g_{iso} values for more polar, protic solvents is well reproduced by the calculations. Furthermore, a noticeable decrease in Δg_{iso} was found in the experiments on the DTBNO radical in acetonitrile (+3651 ± 10 ppm), methanol (+3471 ± 20 ppm) and water (+3241 ± 10 ppm). As expected, this was not recovered in the calculations, where almost constant values of Δg_{iso} were calculated for these three solvents (Table 2). This finding is due to the well-known incapability of continuum models to incorporate hydrogen bonding and was demonstrated already by Rinkevicius et al.[24] However, it will be shown in the next section that the computed *g*-values can be drastically improved by using the supermolecule approach in combination with the COSMO continuum model.

A comparison of the BP and B3LYP results with the available experimental isotropic *g*-values showed good performance for both density functionals as is known from many computational studies. Better results were obtained in this work with the B3LYP hybrid functional. Comparing our study and the work of Rinkevicius et al.[24] with the experimental data shows that our B3LYP calculations yielded typically the overall best agreement between theory and experiment with deviations less than 60 ppm relative to the experimental values for solvents such as TCL, toluene, or acetonitrile.

COSMO Calculations for Systems with Explicit Solvent Molecules. It is evident from Tables 1 and 2 that large differences remain between the calculated and measured isotropic *g*-shifts for protic solvents. This can be explained by the fact that a continuum model like COSMO is not able to describe hydrogen bonding between solvent molecules and the radicals, and their impact on the *g*-values. The consequence is an overestimation of the *g*-shifts, as was found in all calculations with water (Tables 1 and 2). The supermolecule approach can overcome this problem and is demonstrated here for water and methanol. In both cases, one, two, and three solvent molecules were coordinated to the nitroxide group. The radical−solvent complexes were completely geometry optimized with and without using the COSMO approach. The obtained structures of the DPNO radical solvent complexes in the continuum are shown in Figure 3. It can be seen that the inclusion of one or two water molecules led to the formation of one or two strong H-bonds to the nitroxide oxygen atom, whereby the model system with two water molecules can be regarded as most intuitive. These two water molecules can be attributed to the first solvation shell, whereas a third water molecule, in contrast, is involved in a H-bond to one of the other water molecules and can be regarded as a single solvent molecule of the second solvation shell. Table 3 shows the *g*-shifts for the DPNO radical with explicit solvent molecules and compares the results of the calculations employing (a) gas-phase optimized supermolecules and (b) solvent optimized structures (COSMO). It can be seen that both approaches lead to smaller Δg_{xx} shifts for every additional solvent molecule. Considering water, good agreement between experiment ($\Delta g_{iso} = 2761 \pm 10$ ppm) and calculation ($\Delta g_{iso} = 2865$ ppm) was obtained in the B3LYP calculation for the DPNO/2 water model including the COSMO approach (Figure 3). In conclusion from Table 3, a combination of both strategies, the use of continuum models and the supermolecule approach is of advantage.

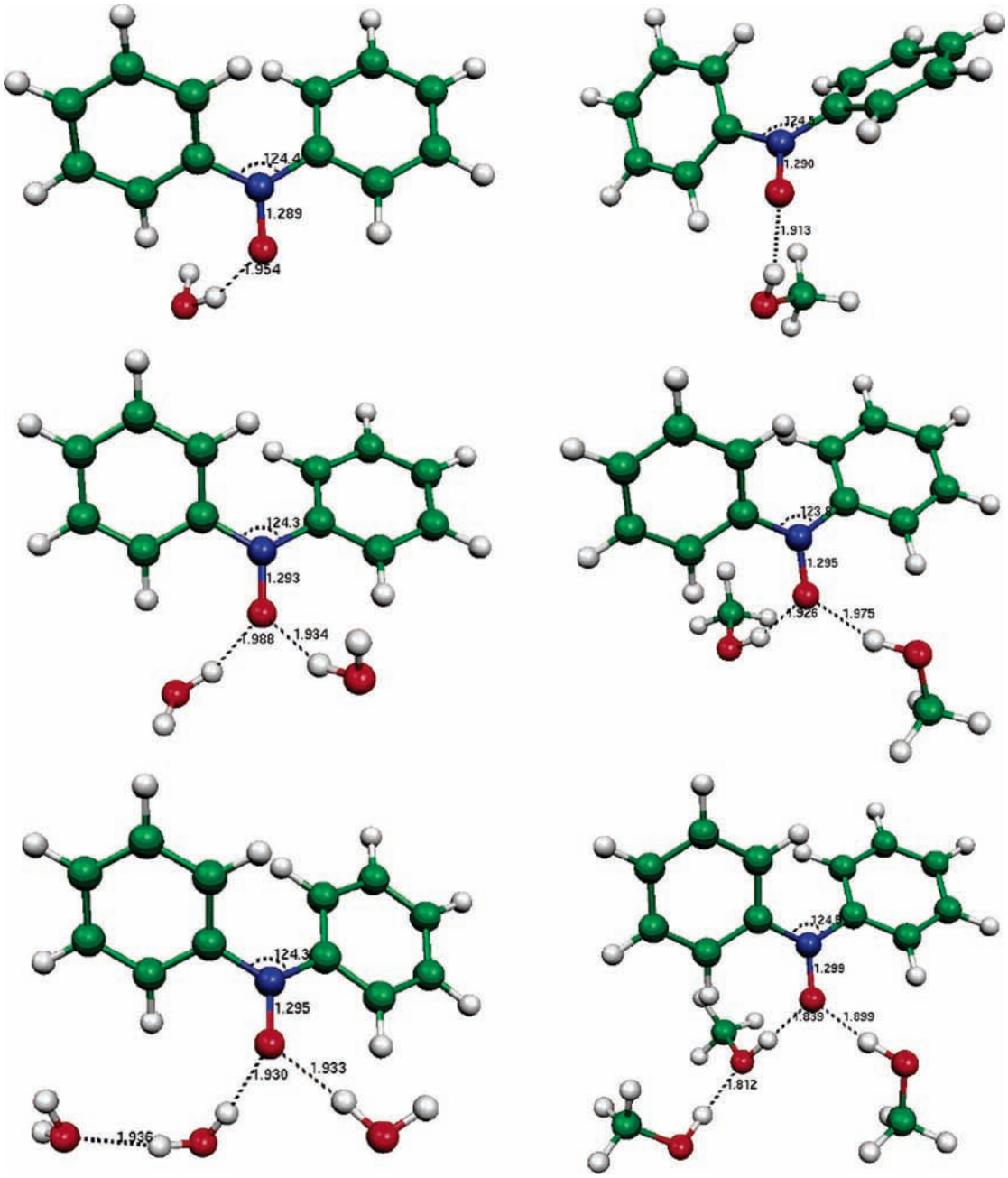

Figure 3. DPNO radical in coordination with explicit solvent molecules (one, two and three water or methanol molecules). Two solvent molecules form H-bonds to the nitroxide oxygen atoms, and the third solvent molecule is hydrogen bonded to another solvent molecule. The COSMO model was used in the geometry optimization ($\epsilon = 80.4$ for water and $\epsilon = 32.63$ for methanol).

For the DPNO radical in methanol, the COSMO calculations without explicit solvent molecules gave already much better agreement between theory and experiment than in the case of water (Table 1) due to the fact that rather similar *g*-shifts were calculated for water and methanol, whereas very different values were measured in the two solvents. In consequence, the inclusion of explicit methanol molecules in the calculations gave no general improvement of the data but resulted in an underestimation of the experimental Δg_{iso} shift (Table 3). Employing the B3LYP functional and the COSMO approach, we found very good agreement between theory ($\Delta g_{iso} = 3110$ ppm) and experiment ($\Delta g_{iso} = 3181 \pm 10$ ppm) for the model system with one explicit methanol molecule. Also in the work of Rinkevicius et al., the best agreement between theory and experiment was found for the nitric oxide radical in coordination with a single methanol molecule.[24] This finding is somewhat counterintuitive but is further supported by the work of Owenius et al.,[47] where it was concluded that on average methanol forms only one H-bond to the investigated nitric oxide spin label. Considering low-temperature magnetic resonance studies on the benzosemiquinone radical anion, very similar *g*-values were obtained in methanol and water,[76] in agreement with DFT calculations.[22] The calculated DPNO/methanol structures were very similar to those of the water solvent case: one or two strong H-bonds were found to be formed between the methanol molecules and the nitroxide oxygen, and the addition of a third methanol molecules gave an additional H-bond between two solvent molecules. However, in the case of methanol, slightly shorter H-bonds were found (Figure 3).

The results obtained for the DTBNO radical in water and methanol are given in Table 4. In comparison to the DPNO radical, a weaker dependence of the isotropic *g*-shifts on the

TABLE 3: Calculated *g*-Shifts (ppm) for the Diphenyl Nitric Oxide Radical DPNO in Water or Methanol (MeOH) Including Explicit Solvent Molecules[a]

	BP				B3LYP			
solvent	Δg_{xx}	Δg_{yy}	Δg_{zz}	Δg_{iso}	Δg_{xx}	Δg_{yy}	Δg_{zz}	Δg_{iso}
Gas-Phase Calculations with Explicit Solvent Molecules								
DPNO/1H_2O	6447	2632	−79	3000	7092	3076	−122	3349
DPNO/2H_2O	5915	2443	−51	2769	6396	2843	−108	3044
DPNO/3H_2O	5812	2375	−58	2709	6248	2763	−112	2966
DPNO/1MeOH	6463	2632	−40	3018	7098	3056	−105	3350
DPNO/2MeOH	5940	2457	−40	2786	6408	2830	−108	3043
DPNO/3MeOH	5860	2367	−62	2722	6311	2735	−116	2976
COSMO Calculations with Explicit Solvent Molecules[b]								
DPNO/1H_2O	5986	2535	−57	2821	6448	2945	−99	3098
DPNO/2H_2O	5599	2359	−50	2636	5959	2734	−98	2865
DPNO/3H_2O	5462	2414	−171	2568	5891	2774	−200	2822
DPNO/1MeOH	6001	2543	−36	2836	6464	2932	−92	3101
DPNO/2MeOH	5545	2374	−26	2631	5897	2718	−94	2840
DPNO/3MeOH	5340	2260	+12	2537	5661	2602	−59	2735

[a] In the experiments, Δg_{iso} shifts of +2761 ± 10 and +3181 ± 10 ppm were found for the DPNO radical in water and methanol, respectively.[40] [b] Solvent optimized structures were employed for the **g**-tensor calculations.

TABLE 4: Calculated *g*-Shifts (ppm) for the *tert*-Butyl Nitric Oxide Radical DTBNO in Water or Methanol Including Explicit Solvent Molecules[a]

	BP				B3LYP			
solvent	Δg_{xx}	Δg_{yy}	Δg_{zz}	Δg_{iso}	Δg_{xx}	Δg_{yy}	Δg_{zz}	Δg_{iso}
Gas-Phase Calculations with Explicit Solvent Molecules								
DTBNO/1H_2O	6231	3596	−205	3207	6833	3931	−231	3511
DTBNO/2H_2O	5968	3394	−206	3052	6533	3730	−232	3344
DTBNO/3H_2O	5713	3438	−195	2986	6207	3749	−222	3244
DTBNO/1MeOH	6149	3570	−214	3168	6742	3888	−242	3463
DTBNO/2MeOH	5986	3341	−149	3059	6484	3663	−197	3317
DTBNO/3MeOH	5826	3360	−191	2998	6221	3659	−225	3218
COSMO Calculations with Explicit Solvent Molecules[b]								
DTBNO/1H_2O	6032	3497	−203	3109	6527	3817	−230	3371
DTBNO/2H_2O	5838	3290	−156	2991	6276	3609	−198	3229
DTBNO/3H_2O	5537	3360	−197	2900	5964	3664	−225	3134
DTBNO/1MeOH	5981	3495	−214	3087	6473	3799	−243	3343
DTBNO/2MeOH	5779	3264	−178	2955	6215	3576	−216	3191
DTBNO/3MeOH	5744	3332	−192	2961	6112	3626	−225	3171

[a] In the experiments, Δg_{iso} shifts of +3241 ± 10 and 3471 ± 20 ppm were found for the DTBNO radical in water and methanol, respectively.[45] [b] Solvent optimized structures were employed for the **g**-tensor calculations.

number of coordinated solvent molecules was found. Good agreement between theory and experiment can be reported again for the B3LYP calculations on the supermolecules based on solvent optimized structures.

A final comparison of our calculated isotropic *g*-values with the available experimental data is given in Table 5. It includes only the results of our B3LYP calculations because they gave better *g*-shifts than the BP functional. For the aprotic solvents, the pure COSMO results are given, whereas for water and methanol, the data of the model systems with two explicit solvent molecules are shown. The small remaining deviations between the calculated isotropic *g*-shifts employing the IGLO-II basis set and the experimental values are close to the estimated errors due to the incompleteness of the basis set. This encouraged us to repeat these calculations with the IGLO-III basis set, augmented by one diffuse function for every element. The data are likewise given in Table 5 and show a noticeable improvement in the results, as is evident from the RMS deviations between theory and experiment. The only critical point is the methanol case. Here, the intuitive model system

TABLE 5: Comparison of Calculated and Measured Isotropic *g*-Shifts (ppm) for the DPNO and DTBNO Radicals Employing the B3LYP Hybrid Functional and the COSMO Approach and Solvent Optimized Geometries[a]

	IGLO-II literature[b]	IGLO-II this work	IGLO-IIId this work	exptl
		DPNO		
TCL	3573	3525	3454	3401 ± 10
methanol	2921	2840	2843	3181 ± 10
water	2933	2865	2825	2761 ± 10
		DTBNO		
TCL	3858	3705	3768	3751 ± 20
toluene	3851	3701	3764	3741 ± 10
acetone	3757	3614	3671	3721 ± 50
acetonitrile	3751	3596	3651	3651 ± 10
methanol	3401	3191	3278	3471 ± 20
water	3344	3229	3294	3241 ± 10
RMSD[c]	122	80	44	

[a] The model systems with water and methanol contain two solvent molecules. [b] Values from Rinkevicius et al.[24] [c] Root-mean-square deviation between theory and experiment for all data from Table 5, except methanol.

TABLE 6: Calculated Isotropic *g*-Shifts Δg_{iso} (ppm) for the DTBNO and DPNO Radicals in Different Solvents, Employing the D-COSMO-RS Approach and Solvent Optimized Geometries

	BP IGLO-II	BP IGLO-IIId	B3LYP IGLO-II	B3LYP IGLO-IIId	exptl
DPNO in acetone	+3092	+3035	+3449	+3364	
DPNO in methanol	+2956	+2870	+3259	+3138	3181 ± 10
DPNO + 2MeOH in methanol	+2619	+2620	+2827	+2824	3181 ± 10
DPNO in water	+2780	+2668	+3029	+2888	2761 ± 10
DPNO + 2H_2O in water	+2534	+2482	+2743	+2685	2761 ± 10
DTBNO in acetone	+3333	+3420	+3668	+3726	3721 ± 50
DTBNO in methanol	+3235	+3315	+3534	+3574	3471 ± 20
DTBNO + 2MeOH in methanol	+2944	+3047	+3175	+3262	3471 ± 20
DTBNO in water	+3172	+3245	+3433	+3476	3241 ± 10
DTBNO + 2H_2O in water	+2949	+3027	+3176	+3240	3241 ± 10

with two explicit solvent molecules is obviously not very well suited and was therefore excluded from the calculation of the RMSD values. Better agreement between theory and experiment was achieved for the model systems with three (water) and one (methanol) explicit solvent molecules. However, the choice of such model systems appears to be somewhat empirical.

D-COSMO-RS Calculations. The extension of COSMO to real solvents (D-COSMO-RS) was applied for both radicals in water, methanol and acetone. For water and methanol, model systems without and with two explicit solvent molecules were chosen. In general, the results in Table 6 show noticeable changes in the calculated g_{iso} shifts in comparison to the pure COSMO results. In many cases, the agreement between theory and experiment is improved. Typically, better results were obtained with the B3LYP functional. Employing this hybrid method in combination with the large basis set IGLO-IIId, deviations of 43 and 103 ppm (DPNO and DTBNO in methanol), and of 127 and 235 ppm (DPNO and DTBNO in water) between theory and experiment were obtained for the model systems without explicit solvent molecules. Considering the drastically reduced computational effort for the D-COSMO-RS method in comparison to the supermolecule approach, this is a remarkable result.

To obtain more insight into the D-COSMO-RS results, a detailed comparison of spin densities, orbital energies and **g**-tensor contributions is given for the DPNO radical in water

TABLE 7: Comparison of Spin Densities, Orbital Energies (eV), and g-Tensor Contributions (Relativistic Mass Correction RMC, Diamagnetic Spin−Orbit DSO, and Paramagnetic Spin−Orbit PSO Contributions) of the DPNO Radical in Water, Obtained from COSMO and D-COSMO-RS and from COSMO Employing Additionally the Supermolecule Approach (B3LYP/IGLO-II)

	COSMO	D-COSMO-RS	COSMO supermolecule approach[a]
orbital energies (E_h)			
SOMO−1	−7.22	−7.46	−7.31
SOMO	−5.43	−5.77	−5.69
ΔE[b]	1.79	1.69	1.62
g-tensor contributions (ppm)			
$\Delta g_{ii,RMC}$	−274	−269	−269
$\Delta g_{xx,DSO}$	+153	+153	+154
$\Delta g_{xx,PSO}$	+7046	+6261	+6074
$\Delta g_{yy,DSO}$	+213	+205	+176
$\Delta g_{yy,PSO}$	+3203	+3085	+2827
$\Delta g_{zz,DSO}$	+162	+157	+132
$\Delta g_{zz,PSO}$	+20	+32	+39
Mulliken spin populations			
N	+0.36	+0.40	+0.42
O	+0.44	+0.39	+0.35
atomic contributions			
Δg_{xx} (N)	+445	+547	+649
Δg_{yy} (N)	+809	+787	+904
Δg_{zz} (N)	0	0	−2
Δg_{iso} (N)	+418	+445	+517
Δg_{xx} (O)	+6453	+5565	+5309
Δg_{yy} (O)	+2115	+1967	+1716
Δg_{zz} (O)	−53	−54	−52
Δg_{iso} (O)	+2838	+2493	+2325

[a] Model system with two explicit solvent molecules. [b] In a vacuum, an energy difference of 1.91 eV was obtained for the SOMO and SOMO−1 levels.

in Table 7. It can be seen that the D-COSMO-RS method (without explicit water molecules) and the supermolecule COSMO approach (with explicit solvent molecules) give rise to similar changes in all these properties upon H-bonding: (i) Spin density is transferred from the oxygen to the nitrogen atom if H-bonds are formed. (ii) A strong stabilization of the SOMO orbital takes place in comparison to the other doubly occupied orbitals, which leads to smaller *g*-shifts. (iii) The dominating paramagnetic spin−orbit contribution to Δg_{xx} is distinctly reduced upon H-bonding. (iv) The largest atomic contributions to the **g**-tensor clearly stem from the oxygen atom of the nitroxide group, and the changes in the **g**-tensor upon formation of H-bonds can be attributed mainly to this oxygen atom. All these points clearly show that the D-COSMO-RS method is able to correctly describe the effects of hydrogen bonding on the solute.

Figure 4 shows the screening charges of the DPNO radical in water, employing the COSMO correction, the D-COSMO-RS approach, and the supermolecule approach in combination with the COSMO method. In general, such figures can help to identify the strongly interacting sites of the solute with the solvent. Here, positive screening charges (red color) were found at the nitroxide oxygen atom with its negative net charge. The difference plot of the screening charges from COSMO and D-COSMO-RS (Figure 4d) shows that the D-COSMO-RS approach additionally increases the positive screening charges at the nitroxide oxygen atom. This indicates a stronger stabilization of the oxygen lone pairs in the D-COSMO-RS calculations. The same effect is evident from the σ-profiles in Figure 5.

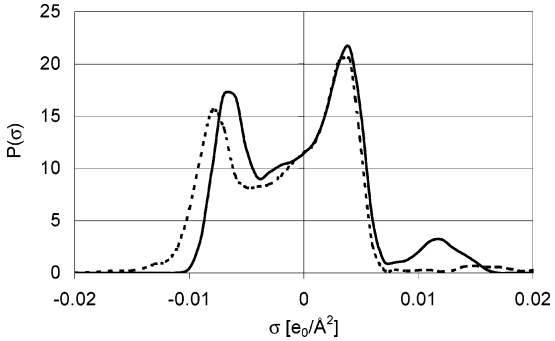

Figure 5. Comparison of the σ-profiles of the DPNO radical in water, obtained with COSMO (straight line) and D-COSMO-RS (dotted line). The diagram shows the number of segments P(σ) with a certain screening charge density σ. Employing the D-COSMO-RS approach, the number of positive screening charges is reduced, and they are shifted to higher values. A similar situation is found for the negative screening charge densities at the hydrogen atoms.

The D-COSMO-RS approach can save a large amount of computational time by neglecting explicit solvent molecules, and it removes the somewhat arbitrary decision of how many solvent molecules have to be included in which conformations in these studies. The D-COSMO-RS calculations have a considerable potential for further studies that cover solvent effects. The only drawback is the σ potential coefficients must be available for every solvent of interest. However, the necessary data can be readily generated from COSMOtherm calculations.

5. Summary and Conclusions

In the present work, we have investigated the effect of solvation on electronic **g**-tensors by studying two nitric oxide radicals. The solvents were modeled employing the COSMO continuum model[11] and the supermolecule approach in case of protic solvents. The **g**-tensor was calculated as a mixed second-derivative with respect to the external magnetic field and the electron magnetic moment, employing the coupled perturbed Kohn−Sham equations.[51] Three different effects of the solvents on the *g*-values were found, which are (a) electrostatic contributions, (b) contributions from hydrogen bonding, and (c) an altered geometry of the solute in the solvent.

We have shown that the electrostatic effects of a solvent can be well described by the COSMO continuum model; that is, very good agreement between theory and experiment can be

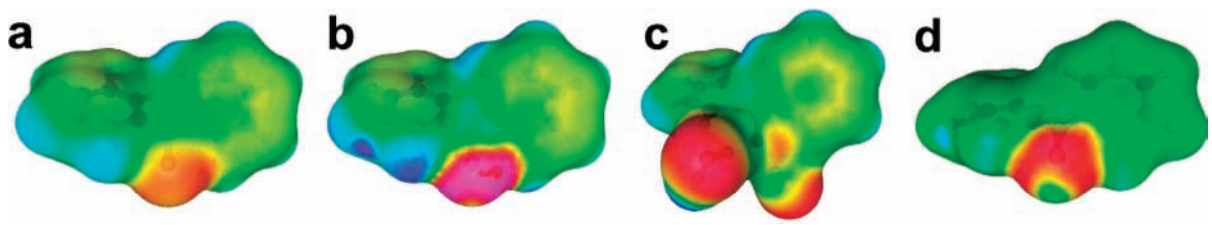

Figure 4. Visualization of the screening charges on the COSMO surface obtained for the DPNO radical in water. The plots were generated by employing (a) the COSMO correction, (b) the D-COSMO-RS approach, (c) the supermolecule approach in combination with the COSMO method, and (d) a difference plot of the screening charges from COSMO and D-COSMO-RS. Positive screening charges are given in red.

reported for aprotic solvents of different polarity. Hereby, the influence of the COSMO approach on the geometrical parameters was found to be small. In general, a more polar surrounding with a larger dielectric constant led to smaller g_{iso} values in the calculations, in agreement with the experimental trends. It was shown that especially the Δg_{xx} shift, pointing along the NO bond, reacts most sensitively on the surrounding.

In case of protic solvents such as methanol or water, the inclusion of explicit solvent molecules, which form H-bonds to the nitric oxide radicals, was necessary to obtain similar good agreement between theory and experiments. Otherwise, the isotropic *g*-shifts are noticeably overestimated in the calculations. Furthermore, a combination of both, the use of a continuum model and of the supermolecule approach, as suggested for instance by Ciofini et al.,[23] was shown to be of advantage in the case of protic solvents.

The extension of the COSMO method to real solvents (D-COSMO-RS) was used in this work for the first time for the calculation of electronic **g**-tensors.[37] It was found to work very well for the calculations of *g*-shifts. Especially the fact that it can model the influence of protic solvents on electronic *g*-shifts without using a supermolecule approach makes it to a very interesting extension to the common dielectric continuum models. Furthermore, the computational effort is identical to that of a standard COSMO calculation, which in our implementation only adds an overhead of ~5% (hybrid functionals) to ~30% (GGA functionals) to the cost of a gas-phase calculation. The D-COSMO-RS method is in addition also well suited for improving the calculated data obtained for aprotic systems. This was shown for acetone, where the D-COSMO-RS data from the B3LYP calculations are in better agreement with the experimental data than the results from the pure COSMO calculations.

A comparison of our data with those from a previous, careful theoretical study of Rinkevicius was provided.[24] In both studies, the same systems were investigated, but we applied a different solvent model, spin unrestricted wave functions and a different spin−orbit coupling operator. The comparison of the calculated data with the experimental isotropic *g*-shifts showed better agreement between theory and experiment for our work. We expect this to be mainly the consequence of our improved spin−orbit coupling operator. In particular, the one-center approximation used in the AMFI approach has been shown to introduce errors of the order of about 100 ppm.[58] Because in this work the experimental results are approached to an accuracy better than 100 ppm, the one-center approximation, which is largely avoided within the RI−SOMF(1X) approach, is a factor that limits the achievable accuracy. We also note in passing that in this study the B3LYP hybrid functional was found to give more accurate *g*-values than the BP functional, which is contrary to previous work and might point to some degree of error compensation in previous calculations with the BP functional.

Although only a few solvent molecules (one to three) were explicitly considered in this work, the performance of molecular dynamics simulations is also feasible. The usefulness of such ensembles for the calculation of electronic **g**-tensors was demonstrated, e.g., by Asher et al. in a rather sophisticated study for the benzosemiquinone anion radical in water.[78]

The inclusion of solvent effects in the calculation of spectroscopic properties is an important prerequisite for obtaining quantitative agreement with the experimental results. The large dependency of the electronic *g*-values on the surrounding that was found in this study is also known from theoretical and experimental studies on quinone radical ions in solvents.[22,23,79−81] Investigating protein cofactors, a related problem is the influence of amino acids in the surrounding of nitroxide spin labels on the magnetic resonance data of the radicals. In this context, EPR *g*-values of nitric oxides in protein environments were found to be useful as local probes for the polarity of the surrounding already in theoretical work.[46,47] Furthermore, EPR data can be very valuable to determine, whether H-bonds to the radicals are formed or not. Studies employing spin labels are of special importance in all cases, where the systems are difficult to crystallize and where spectroscopy is the only source of structural information.

Acknowledgment. This work has been supported by the priority program 1137 "Molecular Magnetism" (F.N.) of the DFG and by the Max-Planck Gesellschaft.

References and Notes

(1) Reichardt, C. *Solvents and Solvent Effects in Organic Chemistry*; VCH: Weinheim, 1990.
(2) Car, R.; Parrinello, M. *Phys. Rev. Lett.* **1985**, *55*, 2471−2474.
(3) Altun, A.; Thiel, W. *J. Phys. Chem. B* **2005**, *109*, 1268−1280.
(4) Chu, J. W.; Brooks, B. R.; Trout, B. L. *J. Am. Chem. Soc.* **2004**, *126*, 16601−16607.
(5) Benzi, C.; Crescenzi, O.; Pavone, M.; Barone, V. *Magn. Reson. Chem.* **2004**, *42*, S57−S67.
(6) Lin, H.; Schöneboom, J. C.; Cohen, S.; Shaik, S.; Thiel, W. *J. Phys. Chem. B* **2004**, *108*, 10083−10088.
(7) Tomasi, J. *Theor. Chem. Acc.* **2004**, *112*, 184−203.
(8) Cramer, C. J.; Truhlar, D. G. *Chem. Rev.* **1999**, *99*, 2161−2200.
(9) Tomasi, J.; Persico, M. *Chem. Rev.* **1994**, *94*, 2027−2094.
(10) Miertuš, S.; Scrocco, E.; Tomasi, J. *Chem. Phys.* **1981**, *55*, 117−129.
(11) Klamt, A.; Schüürmann, G. *Perkin. Trans.* **1993**, 799−805.
(12) Pascual-Ahuir, J. L.; Silla, E.; Tomasi, J.; Bonaccorsi, R. *J. Comput. Chem.* **1987**, *8*, 778−787.
(13) Rivail, J.-L.; Rinaldi, D. *Chem. Phys.* **1976**, *18*, 233−242.
(14) Langlet, J.; Claverie, P.; Caillet, J.; Pullman, A. *J. Phys. Chem.* **1988**, *92*, 1617−1631.
(15) Klein, R. A.; Mennuci, B.; Tomasi, J. *J. Phys. Chem. A* **2004**, *108*, 5851−5863.
(16) Mattar, S. M. *J. Phys. Chem. B* **2004**, *108*, 9449−9455.
(17) Engström, M.; Vahtras, O.; Ågren, H. *Chem. Phys. Lett.* **2000**, *328*, 483−491.
(18) Kaupp, M.; Remenyi, C.; Vaara, J.; Malkina, O. L.; Malkin, V. G. *J. Am. Chem. Soc.* **2002**, *124*, 2709−2722.
(19) Neyman, K. M.; Ganyushin, D. I.; Rinkevicius, Z.; Rösch, N. *Int. J. Quantum. Chem.* **2002**, *90*, 1404−1413.
(20) Engström, M.; Himo, F.; Gräslund, A.; Minaev, B.; Vahtras, O.; Ågren, H. *J. Phys. Chem. A* **2000**, *104*, 5149−5153.
(21) Fritscher, J. *Phys. Chem. Chem. Phys.* **2004**, *6*, 4950−4956.
(22) Sinnecker, S.; Reijerse, E.; Neese, F.; Lubitz, W. *J. Am. Chem. Soc.* **2004**, *126*, 3280−3290.
(23) Ciofini, I.; Reviakine, R.; Arbuznikov, A.; Kaupp, M. *Theor. Chem. Acc.* **2004**, *111*, 132−140.
(24) Rinkevicius, Z.; Telyatnyk, L.; Vahtras, O.; Ruud, K. *J. Chem. Phys.* **2004**, *121*, 5051−5060.
(25) Yan, W. Z.; Xue, Y.; Zhu, H.; Zeng, J.; Xie, D. Q. *J. Comput. Chem.* **2004**, *25*, 1833−1839.
(26) Caricato, M.; Mennucci, B.; Tomasi, J. *J. Phys. Chem. A* **2004**, *108*, 6248−6256.
(27) Stoyanov, S. R.; Villegas, J. M.; Rillema, D. P. *J. Phys. Chem. B* **2004**, *108*, 12175−12180.
(28) Pecul, M.; Ruud, K. *Magn. Reson. Chem.* **2004**, *42*, S128−S137.
(29) Ciofini, I. *Magn. Reson. Chem.* **2004**, *42*, S48−S56.
(30) Ciofini, I.; Adamo, C.; Barone, V. *J. Chem. Phys.* **2004**, *121*, 6710−6718.
(31) Saracino, G. A. A.; Tedeschi, A.; D'Errico, G.; Improta, R.; Franco, L.; Ruzzi, M.; Corvaia, C.; Barone, V. *J. Phys. Chem. A* **2002**, *106*, 10700−10706.
(32) Langgard, M.; Spanget-Larsen, J. *J. Mol. Struct. THEOCHEM* **1998**, *431*, 173−180.
(33) Barone, V. *Chem. Phys. Lett.* **1996**, *262*, 201−206.
(34) Kurad, D.; Jeschke, G.; Marsh, D. *Appl. Magn. Reson.* **2001**, *21*, 469−481.
(35) Steinhoff, H. J.; Savitsky, A.; Wegener, C.; Pfeiffer, M.; Plato, M.; Möbius, K. *Biochim. Biophys. Acta Bioenergetics* **2000**, *1457*, 253−262.
(36) Gaffney, B. J.; Marsh, D. *Proc. Natl. Acad. Sci. U.S.A.* **1998**, *95*, 12940−12943.

(37) Klamt, A. *J. Phys. Chem.* **1995**, *99*, 2224−2235.
(38) Takizawa, O.; Yamauchi, J.; Ohya-Nishiguchi, H.; Deguchi, Y. *Bull. Chem. Soc. Jpn.* **1971**, *44*, 3188.
(39) Yamauchi, J.; Nishiguchi, H.; Mukai, K.; Deguchi, Y.; Takaki, H. *Bull. Chem. Soc. Jpn.* **1967**, *40*, 2512−2518.
(40) Kawamura, T.; Matsunami, S.; Yonezawa, T.; Fukui, K. *Bull. Chem. Soc. Jpn.* **1965**, *38*, 1935−1940.
(41) Deguchi, Y. *Bull. Chem. Soc. Jpn.* **1962**, *35*, 598−602.
(42) Deguchi, Y. *Bull. Chem. Soc. Jpn.* **1962**, *35*, 260−264.
(43) Pannell, J. *Mol. Phys.* **1962**, *5*, 291−300.
(44) Deguchi, Y. *Bull. Chem. Soc. Jpn.* **1961**, *34*, 910−916.
(45) Kawamura, T.; Matsunami, S.; Yonezawa, T. *Bull. Chem. Soc. Jpn.* **1967**, *40*, 1111−1115.
(46) Engström, M.; Vaara, J.; Schimmelpfennig, B.; Ågren, H. *J. Phys. Chem. B* **2002**, *106*, 12354−12360.
(47) Owenius, R.; Engström, M.; Lindgren, M.; Huber, M. *J. Phys. Chem. A* **2001**, *105*, 10967−10977.
(48) Ding, Z.; Gulla, A. F.; Budil, D. E. *J. Chem. Phys.* **2001**, *115*, 10685−10693.
(49) Engström, M.; Owenius, R.; Vahtras, O. *Chem. Phys. Lett.* **2001**, *338*, 407−413.
(50) Yagi, T.; Kikuchi, O. *J. Phys. Chem. A* **1999**, *103*, 9132−9137.
(51) Neese, F. *J. Chem. Phys.* **2001**, *115*, 11080−11096.
(52) Patchkovskii, S.; Schreckenbach, G. In *Calculation of NMR and EPR Parameters. Theory and Applications*; Kaupp, M., Bühl, M., Malkin, V. G., Eds.; Wiley-VCH: Weinheim, 2004; pp 505−532.
(53) Malkina, O. L.; Vaara, J.; Schimmelpfennig, B.; Munzarová, M. L.; Malkin, V. G.; Kaupp, M. *J. Am. Chem. Soc.* **2000**, *122*, 9206−9218.
(54) Kaupp, M.; Reviakine, R.; Malkina, O. L.; Arbuznikov, A.; Schimmelpfennig, B.; Malkin, V. G. *J. Comput. Chem.* **2002**, *23*, 794−803.
(55) Hess, B. A.; Marian, C. M.; Wahlgren, U.; Gropen, O. *Chem. Phys. Lett.* **1996**, *251*, 365−371.
(56) Schimmelpfennig, B.; Maron, L.; Wahlgren, U.; Teichteil, C.; Fagerli, H.; Gropen, O. *Chem. Phys. Lett.* **1998**, *286*, 267−271.
(57) Vahtras, O.; Engstrom, M.; Schimmelpfennig, B. *Chem. Phys. Lett.* **2002**, *351*, 424−430.
(58) Neese, F. *J. Chem. Phys.* **2005**, *122*, 204107.
(59) Berning, A.; Schweizer, M.; Werner, H. J.; Knowles, P. J.; Palmieri, P. *Mol. Phys.* **2000**, *98*, 1823−1833.
(60) Parr, R. G.; Yang, W. T. *Density-Functional Theory of Atoms and Molecules*; Oxford University Press: Oxford, NY, 1994.
(61) Klamt, A.; Jonas, V.; Bürger, T.; Lohrenz, J. C. W. *J. Phys. Chem. A* **1998**, *102*, 5074−5085.
(62) Neese, F. ORCA − an ab initio, Density Functional and Semiempirical Program Package, Version 2.4, Max-Planck Institut für Bioanorganische Chemie, Mülheim an der Ruhr, Germany, 2004.
(63) Eckert, F.; Klamt, A. *AIChE J.* **2002**, *48*, 369−385.
(64) Eckert, F.; Klamt, A. COSMO*therm*, Version C2.1, Release 01.04. Cosmo*logic* GmbH & Co. KG, Leverkusen, Germany, 2004.
(65) Becke, A. D. *J. Chem. Phys.* **1993**, *98*, 5648−5652.
(66) Lee, C. T.; Yang, W. T.; Parr, R. G. *Phys. Rev. B* **1988**, *37*, 785−789.
(67) Hehre, W. J.; Ditchfield, R.; Pople, J. A. *J. Chem. Phys.* **1972**, *56*, 2257−2261.
(68) Hariharan, P. C.; Pople, J. A. *Theor. Chim. Acta* **1973**, *28*, 213−222.
(69) Becke, A. D. *Phys. Rev. A* **1988**, *38*, 3098−3100.
(70) Perdew, J. P. *Phys. Rev. B* **1986**, *34*, 7406.
(71) Perdew, J. P. *Phys. Rev. B* **1986**, *33*, 8822−8824.
(72) Kutzelnigg, W.; Fleischer, U.; Schindler, M. In *NMR Basic Principles and Progress*; Diehl, P., Fluck, E., Günther, H., Kosfeld, R., Seelig, J., Eds.; Springer: Heidelberg, 1990; p 165.
(73) Luzanov, A. V.; Babich, E. N.; Ivanov, V. V. *J. Mol. Struct. THEOCHEM* **1994**, *117*, 211−220.
(74) Stone, A. J. *Mol. Phys.* **1963**, *6*, 509−515.
(75) Stone, A. J. *Mol. Phys.* **1964**, *7*, 311.
(76) Flores, M.; Isaacson, R. A.; Calvo, R.; Feher, G.; Lubitz, W. *Chem. Phys.* **2003**, *294*, 401−413.
(77) Knüpling, M.; Törring, J. T.; Un, S. *Chem. Phys.* **1997**, *219*, 291−304.
(78) Asher, J. R.; Doltsinis, N. L.; Kaupp, M. *J. Am. Chem. Soc.* **2004**, *126*, 9854−9861.
(79) Burghaus, O.; Plato, M.; Rohrer, M.; Möbius, K.; MacMillan, F.; Lubitz, W. *J. Phys. Chem.* **1993**, *97*, 7639−7647.
(80) Nimz, O.; Lendzian, F.; Boullais, C.; Lubitz, W. *Appl. Magn. Reson.* **1998**, *14*, 255−274.
(81) Teutloff, C.; Hofbauer, W.; Zech, S. G.; Stein, M.; Bittl, R.; Lubitz, W. *Appl. Magn. Reson.* **2001**, *21*, 363−379.